RSC Advances

ROYAL SOCIETY OF CHEMISTRY

www.rsc.org/advances

RSC Advances

ARTICLE

Fabrication and characterization of Ag_2CO_3/SnS_2 composites with enhanced visible-light photocatalytic activity for the degradation of organic pollutants †

Received 00th January 2015,
Accepted 00th January 2015

DOI: 10.1039/x0xx00000x

www.rsc.org/

Jin Luo,* Xiaosong Zhou, Jinquan Zhang, Zhihua Du

Ag_2CO_3/SnS_2 composite photocatalysts with different Ag_2CO_3 contents were fabricated by a facile and efficient chemical precipitation method. The as-prepared samples were characterized by scanning electron microscopy, X-ray diffraction, X-ray photoelectron spectroscopy, UV-Vis diffuse reflectance spectroscopy and photoluminescence spectroscopy. The Ag_2CO_3/SnS_2 photocatalyst displayed enhanced photocatalytic activity for the photocatalytic degradation of methyl orange (MO) under visible light irradiation (λ>420 nm), and the optimum photocatalytic activity of Ag_2CO_3/SnS_2 at a weight content of 2.0% Ag_2CO_3 for the degradation of MO was 6.22 and 1.65 times as high as that of pure Ag_2CO_3 and SnS_2, respectively. Such an enhanced photocatalytic performance was predominantly ascribed to the synergistic effect between Ag_2CO_3 and SnS_2, which effectively facilitated interfacial charge transfer and improved photogenerated electron-hole pairs separation efficiency. Furthermore, the superoxide radical anions ($\cdot O_2^-$) and holes (h^+) were considered as the main reactive species during the photodegradation process, and a synergistic photocatalysis mechanism between Ag_2CO_3 and SnS_2 was proposed based on the experimental results.

Introduction

Semiconductor photocatalysis has aroused a great deal of concern due to it represents a promising technology for solving the growing energy and environmental pollution by utilizing abundant sunlight.[1] Although conventional TiO_2 is still most widely investigated because of its high photocatalytic activity and stability, non-toxicity, and low cost,[2] it can only be excited under UV light (ca. 4% of the solar spectrum) irradiation due to its large band gap (3.2 ev for anatase TiO_2),[3] so it can not make full use of sunlight and has hindered practical applications. In order to utilize solar energy more efficiently, it is one of the key objectives to develop visible light (ca. 45% of the solar spectrum)[4] active photocatalysts for practical applications of photocatalysis technology.

Up to now, many attempts have been devoted to finding and designing visible light active photocatalysts, such as graphitic carbon nitride,[5] Ag_3PO_4,[6] Ag_2CO_3,[7] $AgSbO_3$,[8] AgCl,[9] BiOX (X=Cl, Br, and I),[10] Bi_2WO_6,[11] $BiVO_4$,[12] Cu_2O,[13] CdS,[14] and SnS_2,[15] etc. Among them, Ag_2CO_3, as a novel high-efficiency visible light driven photocatalyst, has been recognized as one of the most promising photocatalysts for the degradation of various organic dyes because of its high utilization rate of visible light.[16] Unfortunately, Ag_2CO_3 greatly suffers from poor stability in practical applications due to it usually undergo photocorrosion during the photocatalysis process, which caused the serious deactivation.[17] To solve this problem, Ag_2CO_3 coupling with other semiconductors with matching band potential to form a heterojunction at the interface, such as Ag_2O/Ag_2CO_3,[17b] $Ag_2CO_3/g\text{-}C_3N_4$,[16a] $AgBr/Ag_2CO_3$,[16b] AgI/Ag_2CO_3,[18] Ag_2CO_3/ZnO,[19] Ag_2CO_3/TiO_2,[20] is proven to be an effective strategy for improving the photocatalytic activity and stability under visible light irradiation, because the formation of well-defined junction effectively facilitates charge transfer and suppresses the recombination of photogenerated electrons and holes.[1a,16b]

As one of the most important and fascinating metal-sulfide materials, SnS_2 has been investigated and proved to be a relatively efficient and stable visible-light-driven photocatalyst in the treatment of dyes and Cr(VI) in water, because it has a peculiar CdI_2-type layered structure consisting of tin atoms sandwiched between two layers of hexagonally disposed close-packed sulfur atoms, and is non-toxicity, low cost, good stability in acid and neutral aqueous media, as well as oxidative and thermal stability in air.[15,21] However, to the best of our knowledge, no research on the Ag_2CO_3/SnS_2 composite photocatalyst has been reported so far. Fortunately, since the matching band potentials of Ag_2CO_3 and SnS_2, so it gives us an inspiration that SnS_2 can couple with Ag_2CO_3 to form heterojunction Ag_2CO_3/SnS_2 composites.

Herein, we report a novel heterostructured Ag_2CO_3/SnS_2 composite photocatalysts with different content of Ag_2CO_3 by the hydrothermal technique and the in situ precipitation method. The as-prepared Ag_2CO_3/SnS_2 composites exhibit

School of Chemistry and Chemical Engineering, Institute of Physical Chemistry, and Development Center for New Materials Engineering & Technology in Universities of Guangdong, Lingnan Normal University, Zhanjiang 524048, China. E-mail: lj328520504@126.com; Tel/Fax: +86-759-3183205

enhanced visible-light photocatalytic activity for degradation of methyl orange (MO) and rodamine B (RhB) under visible light irradiation (λ>420 nm), which could be attributed to the synergetic effect between Ag_2CO_3 and SnS_2, which effectively facilitated interfacial charge transfer and improved photogenerated electron-hole pairs separation efficiency. Additionally, the possible transferred and separated behaviors of the charge carriers and the photocatalytic mechanisms are discussed.

Experimental

Catalysts synthesis

SnS_2 nanoplates were prepared by a facile hydrothermal method according to a modified reported procedure.[22] Typically, 2.1 g of tin tetrachloride pentahydrate ($SnCl_4 \cdot 5H_2O$) and 3.0 g of thiourea were first dissolved in 70 mL of distilled water with the assistance of ultrasonication for 10 min. The mixture was transferred into a 100 mL of Teflon-lined stainless steel autoclave and heated at 180 ^{o}C for 10 h. The resulting yellow products were collected by centrifugation, washed several times with distilled water and absolute ethanol, then dried at 60 ^{o}C in vacuum for 24 h.

Ag_2CO_3/SnS_2 composites were fabricated through an in situ chemical precipitation method. Typically, first of all, 500 mg as-prepared SnS_2 samples were immersed into 50 mL distilled water. Then, 0.5 milliliters of 0.03 mol L^{-1} $AgNO_3$ was added into the dispersion of SnS_2 under the vigorous stirring. After stirring for 10 min, 0.5 milliliters of 0.015 mol L^{-1} Na_2CO_3 was added dropwise into the dispersion with constant stirring. The mixture was further vigorously stirred at room temperature for 4 h. Finally, the obtained suspensions solution were collected by centrifugation, washed several times with distilled water and absolute ethanol, then dried at 60 ^{o}C in vacuum for 24 h. The obtained products were denoted as Ag_2CO_3(x)/SnS_2, where x% stands for the mass percent of Ag_2CO_3 in Ag_2CO_3/SnS_2 composite. That is to say, the as-prepared samples were also denoted as Ag_2CO_3(1.0wt%)/SnS_2. Moreover, the Ag_2CO_3(2.0wt%)/SnS_2 and Ag_2CO_3(4.0wt%)/SnS_2 were prepared following the similar procedure mentioned above except for different volume of $AgNO_3$ and Na_2CO_3. For comparison, Ag_2CO_3 nanoparticles were prepared following the similar procedure mentioned above in the absence of SnS_2.

Catalysts characterization

X-ray diffraction (XRD) patterns of the as-prepared samples were recorded on an X-ray diffractometer (D/max-IIIA, Japan) using Cu K_a radiation. The surface morphology of the as-prepared samples was examined by a scanning electron microscopy (SEM) (LEO1530VP, LEO Company). The UV-Vis light absorption spectra of the as-prepared samples were obtained from a Hitachi UV-3010 spectrophotometer equipped with an integrating sphere assembly and using the diffuse reflection method and $BaSO_4$ as a reference to measure all the samples. X-ray photoelectron spectroscopy (XPS) analysis was performed with a Krato Axis ultra DLD spectrometer equipped with an AlKα X-ray source, the binding energy was referenced to C 1s peak at 284.6 eV for calibration. Photoluminescence (PL) spectra were measured on an F-7000 Fluorescence spectrohpotometer (Hitachi, Japan).

Photocatalytic tests of catalysts

The photocatalytic performance of the as-prepared samples was evaluated through the photodegradation of MO under visible light. A 500 W Xe-arc lamp equipped with a 420 nm cutoff filter was used as a visible light source. In a typical photocatalytic measurement, suspension including the photocatalyst (50 mg) and MO solution (150 mL, 10 mg L^{-1}) was laid in a 250 mL cylindrical quartz reactor equipped with a water circulation facility. Before irradiation, the reaction suspension was ultrasonicated for 5 min and stirred in the dark for 60 min to ensure the equilibrium of adsorption and desorption. During the photocatalytic tests, 5 mL of the suspension was obtained at a given time intervals, followed by centrifugation at 10000 rpm for 10 min to remove the photocatalyst. The concentration of the remaining MO was measured by its absorbance (A) at 465 nm with a Hitachi UV-3010 spectrophotometer. The degradation ratio of MO can be calculated by $X=(A_0-A_t)/A_0\times100\%$, where A_0 and A_t are the concentration of MO before illumination and after illumination time t.

Results and discussion

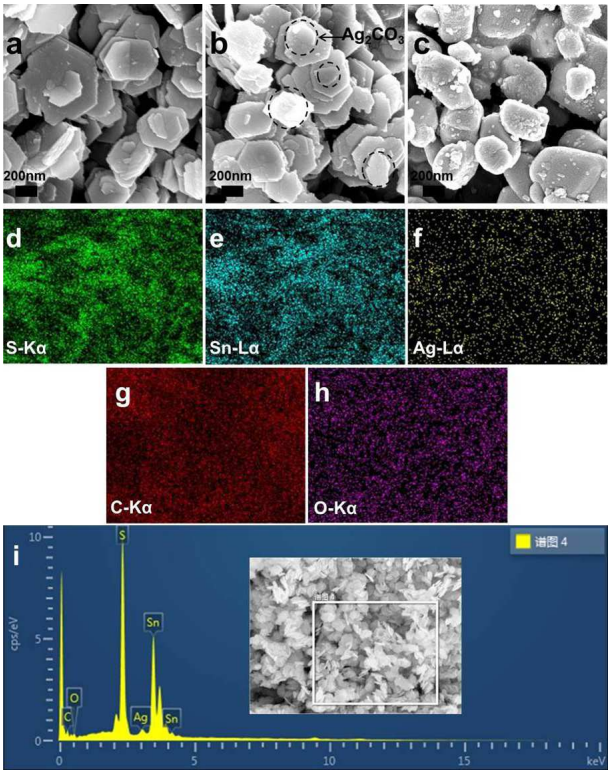

Fig. 1 SEM (a-c) images of SnS_2 (a), Ag_2CO_3(2.0wt%)/SnS_2 (b) and Ag_2CO_3 (c), and elemental mapping images (d-h) and EDS (i) of Ag_2CO_3(2.0wt%)/SnS_2 composite.

Fig. 1 depicts the SEM images of the as-prepared samples. As shown in Fig. 1a, the morphology of pure SnS_2 is composed of stacked hexagonal nanoplates with a diameter of 300-600 nm. Fig. 2c shows the morphology of pure Ag_2CO_3 is composed of microcuboids with a length of 0.3-1.0 μm. Fig. 2b displays the morphology of Ag_2CO_3(2.0wt%)/SnS_2 composite is similar to that of SnS_2, and amounts of Ag_2CO_3 microcuboids are stacked and dispersed on the surface of the SnS_2 nanoplates. It can be verified further by the elemental mapping images of Ag_2CO_3(2.0wt%)/SnS_2 composite (Fig. 1d-h). As shown in Fig. 1f-h, the Ag, C and O elements are homogeneously distributed in the whole host of Ag_2CO_3(2.0wt%)/SnS_2 composite, indicating that the high dispersed Ag_2CO_3 was loaded over SnS_2 nanoplates. Furthermore, the composite samples are purely composed of Ag_2CO_3 and SnS_2 that can be further confirmed from the energy dispersive X-ray spectrum (EDS) as shown in Fig. 1i. It can be unambiguously seen that the Ag_2CO_3(2.0wt%)/SnS_2 composite contains only Ag, O, C, S and Sn elements and no other element or impurity found in the fabricated sample, demonstrating that Ag_2CO_3(2.0wt%)/SnS_2 composite was only composed of both Ag_2CO_3 and SnS_2.

Fig. 2a presents the XRD patterns of the as-prepared samples. It is observed that the sharp and intense diffraction peaks of the as-prepared samples, indicated that all the as-prepared samples are well crystalline. Pure SnS_2 displays five distinct diffraction peaks at 2θ=15.03°, 28.20°, 32.12°, 41.89° and 49.96°, which are in good agreement with (001), (100), (101), (102) and (110) diffraction planes of the hexagonal phase of SnS_2 (JCPDS Card No. 23-0677).[22,23] It is noted that no impurity peaks are detected, which shows that as-prepared SnS_2 are of pure phase. In addition, pure Ag_2CO_3 shows nine distinct diffraction peaks at 2θ=18.55°, 20.54°, 32.59°, 33.67°, 37.07° and 39.58°, which are in good agreement with the (020), (110), (-101), (-130), (200) and (031) diffraction planes of the monoclinic phase of Ag_2CO_3 (JCPDS Card No. 26-0339).[20,24] No impurities can be detected from this pattern of Ag_2CO_3, indicating that the products are of pure phase. Over Ag_2CO_3/SnS_2 composites, no obvious change is observed for the 2θ values of the diffraction peaks of the pure SnS_2, and no characteristic diffraction peaks of Ag_2CO_3 is observed, suggesting that Ag_2CO_3 could exist in a highly dispersed state, it is consistent with the above-mentioned elemental mapping images observation.

The chemical state of the elements in Ag_2CO_3(2.0wt%)/SnS_2 was analyzed by XPS. The high resolution XPS spectra for C 1s, O 1s, S 2p, Sn 3d and Ag 3d for Ag_2CO_3(2.0wt%)/SnS_2 are shown in Fig. 2b-f. The electron binding energies were corrected for specimen charging by referencing the C 1s line to 284.6 eV. Fig. 2b depicts the spectrum of C 1s and the peak positioned at 284.6 eV can be attributed to carbon in Ag_2CO_3.[16a,25] Fig. 2c shows the spectrum of O 1s and the peaks positioned at 531.1 eV and 532.2 eV belong to the O element of Ag_2CO_3 and hydroxyl groups on the surface of Ag_2CO_3, respectively, which is highly consistent with the value reported previously.[3b,16a,18] Fig. 2d displays the spectrum of S 2p and the peaks located at 161.6 eV and 162.7 eV corresponds to S $2p_{3/2}$ and S $2p_{1/2}$, respectively,[26] which can be considered as characteristic of S^{2-} in SnS_2 samples. Fig. 2e displays the spectrum of Sn 3d and the peaks located at 486.8 eV and 495.2 eV belong to Sn $3d_{5/2}$ and Sn $3d_{3/2}$, respectively,[23a,26b] which can be considered as characteristic of Sn^{4+} in SnS_2 samples. Fig. 2f displays the spectrum of Ag 3d and the peaks located at 368.2 eV and 374.2 eV are attributed to Ag $3d_{3/2}$ and Ag $3d_{5/2}$, respectively,[27] which can be considered as characteristic of Ag^+ in Ag_2CO_3 samples. As a consequence, combined with the results of EDS and XPS, it can be confirmed that the coexistence of SnS_2 and Ag_2CO_3 in the Ag_2CO_3/SnS_2 composites.

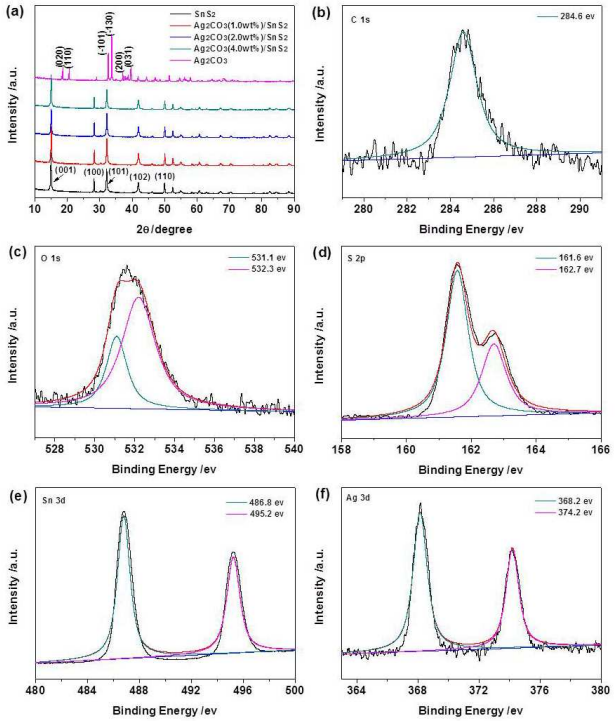

Fig. 2 XRD patterns (a) of the as-prepared samples, C 1s (b), O 1s (c), S 2p (d), Sn 3d (e) and Ag 3d (f) XPS spectrum of the Ag_2CO_3(2.0wt%)/SnS_2 composite.

The light absorption abilities of the as-prepared samples at different light wavelengths were investigated by UV-Vis diffuse reflectance spectroscopy (UV-vis DRS), and the results are recorded in Fig. 3. As can be seen from Fig. 3a, the absorption band edges of pristine SnS_2 and Ag_2CO_3 were estimated to 570 nm and 500 nm, respectively, displayed that the SnS_2 and Ag_2CO_3 both have strong and broader absorption in the visible light region, suggesting their potential capabilities of effectively utilizing visible-light energy. Interestingly, after coupling with Ag_2CO_3, the Ag_2CO_3/SnS_2 composites show a significant enhancement of light absorption, and the absorption intensity increases with the increasing amounts of Ag_2CO_3. It can be attributed to the synergetic effect between

SnS_2 and Ag_2CO_3. Consequently, the combination between SnS_2 and Ag_2CO_3 enhanced the absorption in the visible light region, which may lead to a higher photocatalytic of the Ag_2CO_3/SnS_2 composites. In addition, based on the theory of optical absorption for direct band gap semiconductors, the band gap energy of the as-prepared samples can be calculated through the equation: $\alpha hv=A(hv-E_g)^{n/2}$, where A, α, v, E_g and h are a constant, absorption coefficient, light frequency, band gap energy and Planck constant, respectively.[28] For the value of n, it was determined by the type of optical transition of semiconductors (n=1 for direct transition and n=4 for indirect transition). As previous literatures reported, here the value of n is 1 and 4 for SnS_2 and Ag_2CO_3, respectively.[27b,29] Accordingly, as shown in Fig. 4b, the band gap energy of SnS_2 is estimated to about 2.11 eV according to plots of $(\alpha hv)^2$ versus energy (hv), while the band gap energy of Ag_2CO_3 is estimated to about 2.49 eV according to a plot of $(\alpha hv)^{1/2}$ versus energy (hv). Meanwhile, the conduction band (CB) and valence band (VB) potentials of a semiconductor can be determined using the empirical equation: $E_{CB}=X-E^C-0.5E_g$ and $E_{VB}=E_{CB}+E_g$, where E_{CB} is CB edge potential, E_{VB} is VB edge potential, X is the absolute electronegativity of the semiconductor (the X values for SnS_2 and Ag_2CO_3 are 4.66 eV[30] and 6.02 eV,[20] respectively), E^C is the energy of free electrons on the hydrogen scale (about 4.5 eV vs. NHE) and E_g is the band gap energy of the semiconductor.[28b,31] Therefore, on the basis of the above equations, the VB and CB potentials of Ag_2CO_3 were calculated to be 2.76 eV and 0.27 eV, respectively. Similarly, the VB and CB potentials of SnS_2 were calculated to be 1.21 eV and -0.90 eV, respectively.

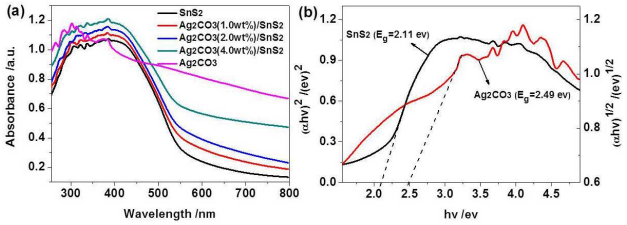

Fig. 3 UV-vis DRS (a) of the as-prepared samples, and plots of $(\alpha hv)^2$ and $(\alpha hv)^{1/2}$ versus energy (b) for the band gap energy of SnS_2 and Ag_2CO_3, respectively.

In order to investigate the effect of Ag_2CO_3 modification, the photoluminescence (PL) spectroscopy of the Ag_2CO_3/SnS_2 composites were performed, because the PL spectra is usually employed to investigate the migration, transfer and recombination processes of photo-generated charge carriers in semiconductors.[16a,32] Generally, a lower PL emission intensity shows a lower recombination rate of photogenerated electron-hole pairs, indicating that more photogenerated electrons and holes can participate in the oxidation and reduction reactions and as a result higher photocatalytic activity is achieved.[33] Fig. 4 presents the PL spectra of the Ag_2CO_3/SnS_2 composites and pure SnS_2 under the excitation wavelength of 325 nm at room temperature. As shown in Fig. 4, it can be seen that the positions of the Ag_2CO_3/SnS_2 composites emission peaks were similar to SnS_2, whereas compared with SnS_2, the PL emission intensities of the Ag_2CO_3/SnS_2 composites obviously decreased. Concretely, the PL emission intensity of Ag_2CO_3/SnS_2 composite decreased at first, reached a maximum and then increased with increasing Ag_2CO_3 content. It indicated that the Ag_2CO_3/SnS_2 composite have a much lower recombination rate of photogenerated charge carriers compared with pure SnS_2, but over-loading Ag_2CO_3 could increase the recombination rate of photogenerated charge carriers. These results clearly indicate that the synergistic effect between Ag_2CO_3 and SnS_2 plays an important role in the effective electron-hole pairs separation that might be a reason for the superior photocatalytic activity of Ag_2CO_3/SnS_2 composites under visible light irradiation. It is noted that the Ag_2CO_3(2.0wt%)/SnS_2 sample showed the weakest emission intensity, meaning that it has the lowest recombination rate of photogenerated charge carriers compared with other composites.

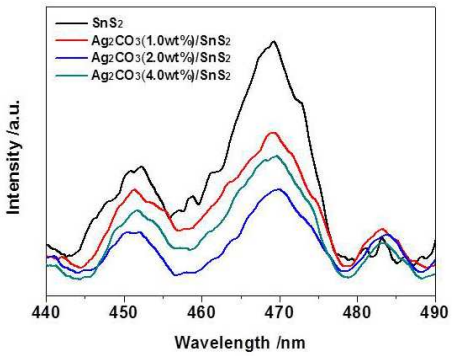

Fig. 4 PL spectra of the as-prepared samples.

The photocatalytic performances of the as-prepared samples were comparatively evaluated by the degradation of methyl orange (MO) under visible light irradiation (λ>420 nm) at room temperature. The experimental results for the photocatalytic activity over the as-prepared samples are presented in Fig. 5. As observed in Fig. 5a, MO molecule is stable under visible light irradiation without using any catalysts because the concentration of MO shows no variations after visible light irradiation for 120 min, indicating that the photolysis of MO is almost negligible in the absence of photocatalyst, and MO is degraded via photocatalytic process. Interestingly, 67 % MO was degraded over Ag_2CO_3(1.0wt%)/SnS_2 composite after visible light irradiation for 120 min, whereas only 20 % and 54 % MO degradation was observed for the same time period in the case of pure Ag_2CO_3 and SnS_2, respectively. Obviously, it can be seen that the photocatalytic performance of SnS_2 is greatly enhanced after coupling with Ag_2CO_3, indicating that Ag_2CO_3 plays an important role in the enhancement of MO degradation. Concretely, the photocatalytic activity of Ag_2CO_3/SnS_2 composite increases first, reaching a maximum around Ag_2CO_3 content of 2.0 wt%, and then decreases with further increasing Ag_2CO_3 content. When the weight ratio of Ag_2CO_3 increased to 2.0 %, the Ag_2CO_3(2.0wt%)/SnS_2 composite exhibited the highest photocatalytic activity, that is to say, 73 % MO is photodegraded after irradiated for 120 min

in the presence of Ag_2CO_3(2.0wt%)/SnS_2, which is 3.7 and 1.4 times as high as that of pure Ag_2CO_3 and SnS_2, respectively. It may be the suitable Ag_2CO_3 can form a good dispersion on the surfaces of SnS_2 nanoplates, which favored the separation and transfer of the photogenerated charge carriers. It can be confirmed from the above-mentioned PL results. However, when the weight ratio of Ag_2CO_3 increased to 4.0 %, the degradation rate of MO decreased to 65 % under the same conditions, but it was much higher compared to the photocatalytic activity of pure SnS_2 and Ag_2CO_3, which indicates that excess Ag_2CO_3 species had a negative effect on the photocatalytic activity. The decrease in the photocatalytic activity can be explained by following reasons: (1) The excess Ag_2CO_3 may act as a recombination centre, and cover the active sites on the SnS_2 surfaces, and thereby reducing the efficiency of charge separation. (2) At higher Ag_2CO_3 content, there is no strong interfacial charge transfer taking place between isolated Ag_2CO_3 microcuboids and SnS_2 nanoplates, which leads to a relatively low charge separation efficiency.[34]
To quantitatively investigate the reaction kinetics of the MO photocatalytic degradation by the as-prepared samples, the experimental data were fitted by applying a first-order model with a simplified Langmuir-Hinshelwood model[35] as expressed by the formula: $-ln(C/C_o)=kt$. where C_o is the equilibrium concentration of MO after 60 min dark adsorption, C is the MO concentration remaining in the solution at the irradiation time, t is the irradiation time and k is the apparent first-order rate constant.[7,36] As shown in Fig. 5b, the plots of $-ln(C/C_o)$ against the irradiation time (t) are nearly linear, and thus the corresponding the apparent first-order rate constants (k) were calculated. Furthermore, it can be seen that the photodegradation rates of all the Ag_2CO_3/SnS_2 composites are much higher than that of the pure Ag_2CO_3 and SnS_2 under visible light irradiation. Concretely, the apparent first-order rate constants (k) for MO degradation with Ag_2CO_3, SnS_2, Ag_2CO_3(1.0wt%)/SnS_2, Ag_2CO_3(2.0wt%)/SnS_2 and Ag_2CO_3 (4.0wt%)/SnS_2 were estimated to be 0.0018 min^{-1}, 0.0068 min^{-1}, 0.0093 min^{-1}, 0.0112 min^{-1} and 0.0090 min^{-1}, respectively. Remarkably, the rate constant of the Ag_2CO_3(2.0wt%)/SnS_2 composite is 6.22 times and 1.65 times as high as that of pure Ag_2CO_3 and SnS_2 under the same experimental conditions, respectively. These results clearly demonstrate that the Ag_2CO_3/SnS_2 composite photocatalysts system can significantly enhance their photocatalytic activities because of the synergistic effect between Ag_2CO_3 and SnS_2. To further confirm the synergistic effect on the present Ag_2CO_3/SnS_2 system, the photocatalytic experiment over the mechanically mixed Ag_2CO_3(2.0wt%)/SnS_2 sample is also investigated and illustrated in Fig. S1. As shown in Fig. S1, it is clear that the photocatalytic activity of Ag_2CO_3(2.0wt%)/SnS_2 composite is much higher than that of the mechanically mixed Ag_2CO_3(2.0wt%)/SnS_2 sample, suggesting that the efficient charge transfer at their interface, which could be attributed to the heterojunction between Ag_2CO_3 and SnS_2 formed in the Ag_2CO_3/SnS_2 hybrid photocatalyst. This observation implies that intimate interface between Ag_2CO_3 and SnS_2 in heterojunction plays an important role in improving the photocatalytic activity. In addition, to broaden the scope of the catalytic application of Ag_2CO_3/SnS_2 hybrid photocatalysts, the photcatalytic activity in the degradation of rodamine B (RhB) is also investigated and illustrated in Fig. S2-3 because of RhB and MO are two different type of dyes. As shown in Fig. S2, it can be seen that the RhB dye can also be photodegraded efficiently over the Ag_2CO_3/SnS_2 hybrid photocatalysts. It is noteworthy that the Ag_2CO_3(2.0wt%)/SnS_2 exhibited the highest photocatalytic activity for the photodegradation of RhB. That is, the rate constant of the Ag_2CO_3(2.0wt%)/SnS_2 composite for the photodegradation of RhB is 2.3 times and 1.7 times as high as that of pure Ag_2CO_3 and SnS_2 under the same experimental conditions, respectively. Consequently, the Ag_2CO_3(2.0wt%)/SnS_2 composite is the best performing sample and was selected for the following recycling experiments.

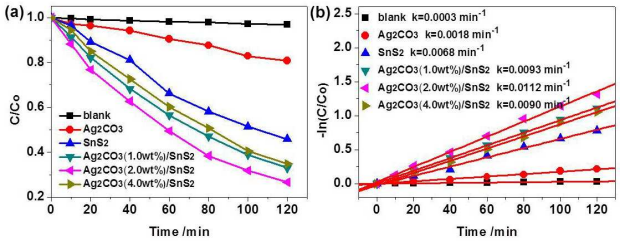

Fig. 5 Photocatalytic activities (a) and first-order kinetic plots (b) for the photodegradation of MO in aqueous solution over the as-prepared samples under visible light irradiation.

It is well known that the recyclability and stability of photocatalyst play an important role in the practical application. Moreover, since Ag_2CO_3 is unstable and can be easily decomposed in photocatalysis process, which can be attributed to the photocorrosion under the visible light irradiation.[16b,37] Therefore, the recycling experiments of Ag_2CO_3(2.0wt%)/SnS_2 composite for the photodegradation of MO was investigated under visible light irradiation. After each run, the recycled catalyst was separated from the aqueous suspension by centrifugation, repeatedly washed by deionized water and ethanol and dried in vacuum at 60 ^oC for 12 h. As can be seen from Fig. 6a, the photocatalytic activity of Ag_2CO_3(2.0wt%)/SnS_2 composite was retained at about 80% of its original activity after four successive experimental runs under the same conditions. The decrease of degradation efficiency under the fourth run may be due to the slight loss of photocatalyst during the cycling reaction. Moreover, Fig. 6b shows the XRD patterns of the Ag_2CO_3(2.0wt%)/SnS_2 composite before and after four experimental run for the photodegradation of MO under visible light irradiation. As shown in Fig. 6b, it can be seen that the XRD pattern of the Ag_2CO_3(2.0wt%)/SnS_2 composite has no obvious changes after four cycles. It is noteworthy that there was no a new weak peak located at 2θ=38.1^o corresponding to the (111) plane diffraction of Ag (JCPDS Card No. 89-3722).[7,37] The results indicated that the Ag_2CO_3(2.0wt%)/SnS_2 composite can be regarded as stable during the photocatalytic degradation of MO under visible light irradiation, which promotes the photocatalyst for its practical application in environmental remediation.

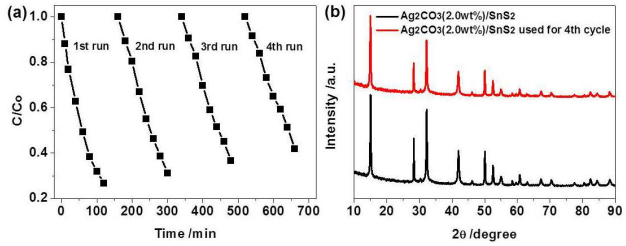

Fig. 6 Recyclability (a) of the Ag_2CO_3(2.0wt%)/SnS_2 composite in four successive experiments for the photocatalytic degradation of MO under visible light irradiation, and the XRD patterns (b) of the Ag_2CO_3(2.0wt%)/SnS_2 composite before and after four consecutive photocatalytic reactions.

It is generally accepted that organic pollutants can be degraded by photocatalytic oxidation processes, in which a series of photoinduced reactive species, such as hydroxyl radical (·OH), hole (h^+) and superoxide radical ($\cdot O_2^-$), are suspected to be involved in the photocatalytic degradation reaction.[32] As a sequence, to elucidate the main reactive species responsible for the photocatalytic degradation of MO over Ag_2CO_3/SnS_2 composite photocatalyst, a series of free radical trapping experiments were employed to scavenge the relevant reactive species. In this investigation, tert-butyl alcohol (t-BuOH), triethanolamine (TEOA) and 1, 4-benzoquinone (BQ) are used as ·OH, h^+ and $\cdot O_2^-$ scavenger, respectively.[2a,38] As illustrated in Fig. 7, after the addition of t-BuOH, the photocatalytic activity of the Ag_2CO_3(2.0wt%)/SnS_2 composite decreases slightly compared to that without scavengers, indicating that ·OH is not the main active species in Ag_2CO_3/SnS_2 composite photocatalytic system. On the contrary, once TEOA or BQ is added, the photocatalytic activity of the Ag_2CO_3(2.0wt%)/SnS_2 composite decreases severely, indicating that h^+ and $\cdot O_2^-$ are the main oxidative species that participate in the photodegradation reaction under visible light irradiation.

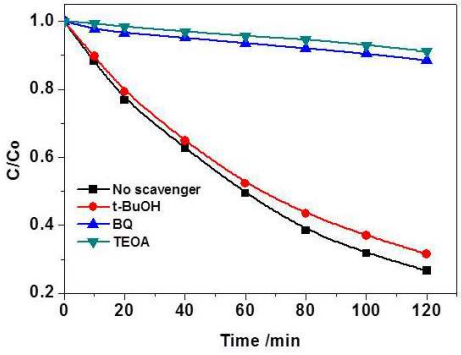

Fig. 7 Effects of various scavengers on the visible light photocatalytic activity of the Ag_2CO_3(2.0wt%)/SnS_2 composite.

On the basis of the above-mentioned experimental results and analysis, the schematic mechanism of the photocatalytic activity of the Ag_2CO_3/SnS_2 composite is proposed and illustrated in Fig. 8. According to the aforementioned calculation results of the band structures, the band gap of Ag_2CO_3 and SnS_2 is 2.49 ev and 2.11 ev, respectively. Therefore, both Ag_2CO_3 and SnS_2 can be excited and generate the photoinduced electron-hole pairs under visible light irradiation. Under normal case, most of electrons-hole pairs recombine rapidly, thus the pure SnS_2 and Ag_2CO_3 have a relative low photocatalytic activity. Fortunately, due to the well-matched overlapping band structures and intimate interfaces of SnS_2 and Ag_2CO_3, the photoinduced electrons on the SnS_2 surfaces can be easily transferred to the CB of Ag_2CO_3 due to the fact that the CB edge potential of SnS_2 is more negative than that of Ag_2CO_3, resulting in accumulation of negative charges in the Ag_2CO_3 region near the junction. Meanwhile, the holes on the VB of Ag_2CO_3 could transfer to the VB of SnS_2 through the closely contacted interfaces due to the fact that the VB edge potential of Ag_2CO_3 is more positive than that of SnS_2, resulting in accumulation of positive charges in the SnS_2 region near the junction. As a result, the internal electric field (*E*) is established between the interfaces (Fig. 8). It is worth mentioning that the inner established electric field at the heterojunction interfaces promoted the migration of photoinduced charge carriers.[34b,39] In such a way, the photoinduced electron-hole pairs are effectively separated because of the synergistic effect between Ag_2CO_3 and SnS_2, which promoted a junction formed between Ag_2CO_3 and SnS_2 interface, resulting in the slow-down recombination photogenerated electron-hole pairs and inducing more charge carriers to participate in photodegradation process, further leading to the enhanced photocatalytic activity. This conclusion can be verified by the above-mentioned PL results. Additionally, the enriched electrons left on the CB of Ag_2CO_3 could be trapped by dissolved oxygen in the reaction solution to form $\cdot O_2^-$, which efficiently protects Ag_2CO_3 to avoid its photoreduction.[17b,34b,40] Consequently, the Ag_2CO_3/SnS_2 composite exhibits relative high photostability. Subsequently, produced $\cdot O_2^-$ would oxidize the MO to CO_2, H_2O and other inorganic molecules, while the holes located on the VB of SnS_2 would also oxidize the MO directly to CO_2, H_2O and other inorganic molecules, This is consistent with our experiment results, the MO degradation rate is decreased obviously in the presence of TEOA or BQ.

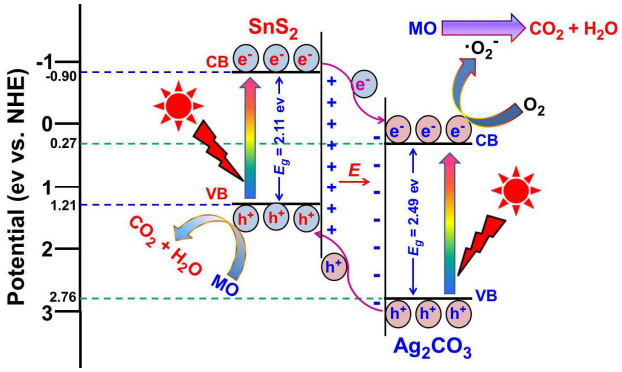

Fig. 8 Schematic illustration of the charge transfer pathway of the Ag_2CO_3/SnS_2 composite catalyst under visible light irradiation.

Conclusions

In summary, a novel visible-light driven Ag_2CO_3/SnS_2 composite photocatalyst has been successfully fabricated by a facile and efficient chemical precipitation method. The Ag_2CO_3/SnS_2 composites displayed enhanced photocatalytic activity for the photocatalytic degradation of methyl orange compared to the single Ag_2CO_3 and SnS_2 under visible light irradiation. Especially, the rate constant of the Ag_2CO_3 (2.0wt%)/SnS_2 composite is 6.22 times as high as that of pure Ag_2CO_3 and 1.65 times larger than that of pure SnS_2, respectively. Such an enhanced photocatalytic performance was predominantly ascribed to the synergistic effect between Ag_2CO_3 and SnS_2, which effectively facilitated interfacial charge transfer and improved photogenerated electron-hole pairs separation efficiency. Moreover, the superoxide radical anions ($\cdot O_2^-$) and holes (h^+) were considered as the main reactive species during the photodegradation process, and a possible photocatalytic mechanism is proposed based on the experimental results. We believe the results presented here provide a new strategy for the rational design of more efficient visible-light driven photocatalysts.

Acknowledgements

This work was supported by Lingnan Normal University Natural Science Foundation for the Ph.D. Start-up Program (ZL1308) and the Guangdong Provincial Natural Science Foundation (No. 2015A030310431, 2015A030313893).

Notes and references

1 a) J. X. Wang, J. Y. Shen, D. L. Fan, Z. S. Cui, X. M. Lü, J. M. Xie, M. Chen, *Mater. Lett.*, 2015, **147**, 8-11; b) J. Wan, L. Sun, J. Fan, E. Z. Liu, X. Y. Hu, C. N. Tang, Y. C. Yin, *Appl. Surf. Sci.*, 2015, **355**, 615-622.

2 a) J. Luo, X. S. Zhou, L. Ma, X. Y. Xu, *RSC Adv.*, 2015, **5**, 68728-68735; b) S. H. Guo, J. X. Bao, T. Hu, L. B. Zhang, L. Yang, J. H. Peng, C. Y. Jiang, *Nanoscale Res. Lett.*, 2015, **10**, 1-8.

3 a) G. P. Dai, J. G. Yu, G. Liu, *J. Phys. Chem. C*, 2012, **116**, 15519-15524; b) X. X. Yao, X. H. Liu, *J. Hazard. Mater.*, 2014, **280**, 260-268.

4 B. Jin, X. S. Zhou, J. Luo, X. Y. Xu, L. Ma, D. Y. Huang, Z. L. Shao, Z. H. Luo, *RSC Adv.*, 2015, **5**, 48118-48123.

5 X. C. Wang, K. Maeda, A. Thomas, K. Takanabe, G. Xin, J. M. Carlsson, K. Domen, M. Antonietti, *Nat. Mater.*, 2009, **8**, 76-80.

6 D. J. Martin, G. G. Liu, S. J. A. Moniz, Y. P. Bi, A. M. Beale, J. H. Ye, J. W. Tang, *Chem. Soc. Rev.*, 2015, DOI: 10.1039/C5CS00380F.

7 H. Xu, Y. X. Song, Y. H. Song, J. X. Zhu, T. T. Zhu, C. B. Liu, D. X. Zhao, Q. Zhang, H. M. Li, *RSC Adv.*, 2014, **4**, 34539-34547.

8 W. J. Liu, X. B. Liu, Y. H. Fu, Q. Q. You, R. K. Huang, P. Liu, Z. H. Li, *Appl. Catal. B: Environ.*, 2012, **123-124**, 78-83.

9 Z. Z. Lou, B. B. Huang, X. Y. Qin, X. Y. Zhang, H. F. Cheng, Y. Y. Liu, S. Y. Wang, J. P. Wang, Y. Dai, *Chem. Commun.*, 2012, **48**, 3488-3490.

10 J. Li, Y. Yu, L. Z. Zhang, *Nanoscale*, 2014, **6**, 8473-8488.

11 X. N. Liu, Q. F. Lu, C. F. Zhu, S. W. Liu, *RSC Adv.*, 2015, **5**, 4077-4082.

12 H. L. Lin, H. F. Ye, S. F. Chen, Y. Chen, *RSC Adv.*, 2014, **4**, 10968-10974.

13 Y. L. Liu, G. J. Yang, H. Zhang, Y. Q. Cheng, K. Q. Chen, Z. Y. Peng, W. Chen, *RSC Adv.*, 2014, **4**, 24363-24368.

14 L. J. Ma, M. C. Liu, D. W. Jing, L. J. Guo, *J. Mater. Chem. A*, 2015, **3**, 5701-5707.

15 Y. C. Zhang, Z. N. Du, S. Y. Li, M. Zhang, *Appl. Catal. B: Environ.*, 2010, **95**, 153-159.

16 a) Y. F. Li, L. Fang, R. X. Jin, Y. Yang, X. Fang, Y. Xing, S. Y. Song, *Nanoscale*, 2015, **7**, 758-764; b) O. Mehraj, N. A. Mir, B. M. Pirzada, S. Sabir, M. Muneer, *J. Mol. Catal. A: Chem.*, 2014, **395**, 16-24.

17 a) C. X. Feng, G. G. Li, P. H. Ren, Y. Wang, X. S. Huang, D. L. Li, *Appl. Catal. B: Environ.*, 2014, **158-159**, 224-232; b) C. L. Yu, G. Li, S. Kumar, K. Yang, R. C. Jin, *Adv. Mater.*, 2014, **26**, 892-898.

18 C. L. Yu, L. F. Wei, W. Q. Zhou, J. C. Chen, Q. Z. Fan, H. Liu, *Appl. Surf. Sci.*, 2014, **319**, 312-318.

19 C. L. Wu, *Mater. Lett.*, 2014, **136**, 262-264.

20 C. L. Yu, L. F. Wei, J. C. Chen, Y. Xie, W. Q. Zhou, Q. Z. Fan, *Ind. Eng. Chem. Res.*, 2014, **53**, 5759-5766.

21 a) H. Liu, L. Deng, Z. F. Zhang, J. Guan, Y. Yang, Z. F. Zhu, *J. Mater. Sci.*, 2015, **50**, 3207-3211; b) Z. C. Wu, Y. J. Xue, Y. L. Zhang, J. J. Li, T. Chen, *RSC Adv.*, 2015, **5**, 24640-24648; c) W. M. Du, D. H. Deng, Z. T. Han, W. Xiao, C. Bian, X. F. Qian, *CrystEngComm*, 2011, **13**, 2071-2076.

22 L. Y. Mao, J. J. Li, Y. L. Xie, Y. J. Zhong, Y. Hu, *RSC Adv.*, 2014, **4**, 29698-29701.

23 a) Z. Y. Zhang, J. D. Huang, M. Y. Zhang, Q. Yuan, B. Dong, *Appl. Catal. B: Environ.*, 2015, **163**, 298-305; b) J. M. Ma, D. N. Lei, L. Mei, X. C. Duan, Q. H. Li, T. H. Wang, W. J. Zheng, *CrystEngComm*, 2012, **14**, 832-836.

24 N. Mohaghegh, B. Eshaghi, E. Rahimi, M. R. Gholami, *J. Mol. Catal. A: Chem.*, 2015, **406**, 152-158.

25 H. J. Dong, G. Chen, J. X. Sun, Y. J. Feng, C. M. Li, G. H. Xiong, C. D. Lv, *Dalton Trans.*, 2014, 43, 7282-7289.

26 a) Y. C. Zhang, Z. N. Du, K. W. Li, M. Zhang, D. D. Dionysiou, *ACS Appl. Mater. Interfaces*, 2011, **3**, 1528-1537; b) Z. Y. Zhang, C. L. Shao, X. H. Li, Y. Y. Sun, M. Y. Zhang, J. B. Mu, P. Zhang, Z. C. Guo, Y. C. Liu, *Nanoscale*, 2013, **5**, 606-618.

27 a) H. Xu, J. X. Zhu, Y. X. Song, T. T. Zhu, W. K. Zhao, Y. H. Song, Z. L. Da, C. B. Liu, H. M. Li, *J. Alloys Compd.*, 2015, **622**, 347-357; b) N. Tian, H. W. Huang, Y. He, Y. X. Guo, Y. H. Zhang, *Colloids Surf. A: Physicochem. Eng. Aspects*, 2015, **467**, 188-194.

28 a) L. Wang, J. Ding, Y. Y. Chai, Q. Q. Liu, J. Ren, X. Liu, W. L. Dai, *Dalton Trans.*, 2015, 44, 11223-11234; b) L. Y. Huang, Y. P. Li, H. Xu, Y. G. Xu, J. X. Xia, K. Wang, H. M. Li, X. N. Cheng, *RSC Adv.*, 2013, **3**, 22269-22279.

29 a) X. H. Hu, G. S. Song, W. Y. Li, Y. L. Peng, L. Jiang, Y. F. Xue, Q. Liu, Z. G. Chen, J. Q. Hu, *Mater. Res. Bull.*, 2013, **48**, 2325-2332; b) H. J. Dong, G. Chen, J. X. Sun, C. M. Li, Y. G. Yu, D. H. Chen, *Appl. Catal. B: Environ.*, 2013, **134**, 46-54.

30 X. Li, J. Zhu, H. X. Li, *Appl. Catal. B: Environ.*, 2012, **123-124**, 174-181.

31 a) D. Channei, B. Inceesungvorn, N. Wetchakun, S. Ukritnukun, A. Nattestad, J. Chen, S. Phanichphant, *Sci. Rep.*, 2014, **4**, 5757; b) H. Xu, Y. G. Xu, H. M. Li, J. X. Xia, J. Xiong, S. Yin, C. J. Huang, H. L. Wan, *Dalton Trans.*, 2012, 41, 3387-3394.

32 C. C. Han, L. Ge, C. F. Chen, Y. J. Li, X. L. Xiao, Y. N. Zhang, L. L. Guo, *Appl. Catal. B: Environ.*, 2014, 147, 546-553.

33 I. Aslam, C. B. Cao, M. Tanveer, M. H. Farooq, W. S. Khan, M. Tahir, F. Idrees, S. Khalid, *RSC Adv.*, 2015, **5**, 6019-6026.
34 a) D. L. Jiang, J. J. Zhu, M. Chen, J. M. Xie, *J. Colloid Interf. Sci.*, 2014, **417**, 115-120; b) S. Tonda, S. Kumar, V. Shanker, *J. Environ. Chem. Eng.*, 2015, **3**, 852-861.
35 C. S. Turchi, D. F. Ollis, *J. Catal.*, 1990, **122**, 178-192.
36 a) S. Ye, L. G. Qiu, Y. P. Yuan, Y. J. Zhu, J. Xia, J. F. Zhu, *J. Mater. Chem. A*, 2013, 1, 3008-3015; b) H. Y. Chen, L. G. Qiu, J. D. Xiao, S. Ye, X. Jiang, Y. P. Yuan, *RSC Adv.*, 2014, 4, 22491-22496.
37 C. Dong, K. L. Wu, X. W. Wei, X. Z. Li, L. Liu, T. H. Ding, J. Wang, Y. Ye, *CrystEngComm*, 2014, **16**, 730-736.
38 S. W. Zhang, J. X. Li, X. K. Wang, Y. S. Huang, M. Y. Zeng, J. Z. Xu, *ACS Appl. Mater. Interfaces*, 2014, **6**, 22116-22125.
39 D. L. Jiang, L. L. Chen, J. J. Zhu, M. Chen, W. D. Shi, J. M. Xie, *Dalton Trans.*, 2013, **42**, 15726-15734.
40 H. Xu, J. X. Zhu, Y. X. Song, W. K. Zhao, Y. G. Xu, Y. H. Song, H. Y. Ji, H. M. Li, *RSC Adv.*, 2014, **4**, 9139-9147.

Graphical Abstract

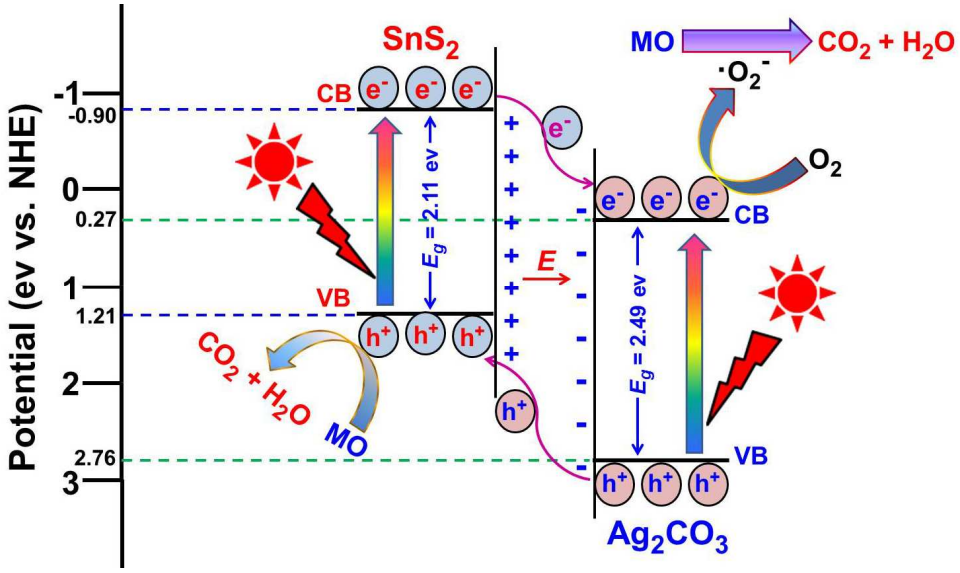

The efficient charge transfer at the interfaces of Ag_2CO_3/SnS_2 composite due to the synergistic effect between Ag_2CO_3 and SnS_2, which formed the inner electric field (E). It effectively facilitated interfacial charge transfer and improved photogenerated electron-hole pairs separation efficiency.